Lab on a Chip

PAPER

View Article Online
View Journal

Cite this: DOI: 10.1039/d6lc00165c

Capillary flow-driven paper-based microfluidic sensor for NDMA detection in water

Prakash Aryal,[a] Jade Manna-Rubenstein,[a] Tessa Whitaker,[a] Eric Brack[b] and Charles S. Henry *[a]

N-Nitrosodimethylamine (NDMA) is a genotoxic nitrosamine that is commonly found in water due to its ready formation from commonly available precursor compounds. Routine monitoring of NDMA in water is challenging due to the need for complex sample preparation and instrumentation. Here, we propose the first example of an NDMA assay on a paper-based microfluidic platform. Moreover, it is the first study to integrate the required photochemical nitrosation reaction directly on-chip, enabling a complete photochemical–colorimetric workflow. The device is constructed with hollow PET capillary channels, double-sided adhesive, and glass fiber/paper pads with immobilized reagents, enabling sample analysis by simply dipping the device into water. On-chip detection of NDMA with sodium 1-naphthol-4-sulfonate is followed by Fe^{2+}- and Co^{2+}-based complexation, producing complementary green and red chromogenic signals. Its user-friendly dip-and-fold operation facilitates on-site, rapid, and high-frequency monitoring. The Fe^{2+}- and Co^{2+}-based channels provide linear detection ranges of 0–100 ppm and 0–30 ppm, with limits of detection of 4 ppm and 1.5 ppm, respectively. Interference studies, proper masking strategies, and dual-channel readout ensured high selectivity, while stability tests demonstrated excellent device stability over four weeks. Spike recovery experiments in tap, river, and lake water showed consistent recovery performance with RSD $< 10\%$. This sustainable platform costs less than $0.2 per device, is compatible with smartphone-based readout, and offers a practical alternative to conventional analytical techniques. The findings presented here open possibilities to expand on-chip photochemical reactions in paper-based and other microfluidic systems for the detection of a broader range of contaminants.

Received 19th February 2026,
Accepted 9th May 2026

DOI: 10.1039/d6lc00165c

rsc.li/loc

1. Introduction

N-Nitrosodimethylamine (NDMA) is a volatile, water-soluble *N*-nitrosamine that forms readily from common precursors and acts as a potent genotoxic environmental contaminant.[1] NDMA was first produced on an industrial scale as a byproduct in the manufacturing of unsymmetrical dimethylhydrazine (a liquid rocket propellant). Initially, NDMA was used as an antioxidant, lubricant additive, and polymer softener; but over subsequent decades, NDMA appeared as an unintended contaminant in various manufacturing processes. Most notably, NDMA was found as a nitrosamine impurity in certain pharmaceuticals, prompting major recalls of contaminated Valsartan and other drugs.[2–6] Although NDMA has arisen from a variety of historical and incidental sources, its presence in contemporary drinking water primarily stems from formation as a disinfection byproduct.[7] In the early 2000s, U.S. water treatment systems attempted to improve microbial control and reduce other byproducts such as trihalomethanes by switching disinfectants from free chlorine to chloramines.[8,9] During chloramination, monochloramine and dichloramine react with dimethylamine-containing precursors from quaternary amine polymers, pharmaceuticals, and wastewater-derived organic nitrogen through chloramine substitution, oxidation, and nitrosation steps to form NDMA, which can persist into finished drinking water.[10–13]

Despite being a semi-volatile liquid with limited sorption to organic carbon, NDMA possesses sufficient environmental stability to migrate through different water sources as a persistent contaminant plume.[14,15] Consequently, concern about NDMA exists due to its high mobility in aquatic systems, multiple pathways into water supplies, and severe health effects at extremely low doses.[16,17] NDMA can leach or be transported into surface and groundwater, enabling contamination of drinking water sources far from the original point of release. Toxicologically, NDMA is classified by the U.S. Environmental Protection Agency (EPA) as a probable human carcinogen (Group B2) and by the

[a] *Department of Chemistry, Colorado State University, Fort Collins, CO, 80523, USA. E-mail: Chuck.henry@colostate.edu*
[b] *U.S. Army Combat Capabilities Development Command (DEVCOM)—Soldier Center, Natick, Massachusetts 01760, USA*

International Agency for Research on Cancer (IARC) as "probably carcinogenic to humans" (Group 2A).[16,18] Acute human exposures to high NDMA doses have caused fulminant hepatic failure.[18] Recent epidemiological investigations related to NDMA-contaminated pharmaceuticals examined potential associations with gastric and colorectal cancers, and highlighted concern about long-term systemic exposure even when environmental concentrations are low.[19–21] Chronic low-level exposure is linked to progressive liver injury, hematological abnormalities (*e.g.*, thrombocytopenia), and elevated risks of liver and other cancers. Acute high-dose exposure to NDMA results in nausea, vomiting, headache, jaundice, and fulminant hepatic failure.[18,22,23] Despite these risks, the U.S. EPA has not established a federal Maximum Contaminant Level (MCL) for NDMA in drinking water.

Regular monitoring and testing of NDMA levels in water systems as a preventative public health measure is critical to identify and mitigate contamination before it leads to widespread health crises, much like the decades-long oversight of per- and polyfluoroalkyl substances (PFAS), which were initially dismissed as inert but later revealed as persistent toxins linked to cancers, immune dysfunction, and massive remediation costs exceeding billions.[24–26] Frequent testing enables regulatory bodies and industries to track pollution sources, enforce safety standards, and implement timely remediation efforts. The absence of accessible, affordable, and rapid tools leaves communities vulnerable to undetected chronic exposure, progressive environmental degradation, and increased long-term health and economic burdens.[27]

The gold standard for NDMA quantification in drinking water, EPA Method 521, relies on solid-phase extraction (SPE) of large-volume samples followed by gas chromatography-tandem mass spectrometry (GC-MS/MS).[28–30] This workflow requires long (up to 14-day) sample holding times, specialized instrumentation, extensive sample cleanup, and highly trained operators.[31] Other established techniques, including high-performance liquid chromatography with chemiluminescence detection after UV photolysis, GC-MS/MS variants using triple-quadrupole detectors,[32] and liquid chromatography–high-resolution mass spectrometry (LC-HRMS),[33] also require centralized laboratories, incur high analytical costs (~$500–1000 per sample), and involve turnaround times of days to weeks, limiting their suitability for timely field-based decision-making.[34] Emerging alternatives, such as molecularly imprinted polymer (MIP)-based electrochemical sensors,[35] can achieve high sensitivity but depend on costly portable potentiostats, face challenges related to incomplete template removal, and require complex electrode fabrication steps that hinder practical field deployment.[36,37]

Recently, Beard *et al.* introduced a promising colorimetric assay for aqueous NDMA detection based on photochemical nitrosation of a commercial naphtholsulfonate indicator.[38] In their method, NDMA functions as a photodonor under UV irradiation, transferring a nitroso group to the naphtholsulfonate to generate a nitrosated product that subsequently forms a green Fe(II)-complex and red Co(II)-complex, hence establishing a new analytical pathway.[38] However, the quantitative analysis requires a benchtop UV–vis spectroscopy, which limits suitability for point-of-need applications due to the associated instrumentation cost, power requirements, and operational complexity. To the best of our knowledge, no studies have reported a paper-based microfluidic platform for NDMA detection, nor has on-chip photochemistry been demonstrated for microfluidic systems in this context. These limitations underscore the need to bridge the gap with lab-on-a-chip platforms capable of fast, low-cost, and portable NDMA detection suitable for decentralized monitoring.

To address this need, we developed a capillary flow-driven, paper-based microfluidic system coupled with a 3D-printed UV irradiation chamber for NDMA detection in water samples. This platform provides high portability, rapid analysis times, and automated operation. Unlike conventional paper-based devices, our system transports samples through hollow capillary channels within seconds, minimizing sample adsorption to channel walls and ensuring efficient reagent delivery. To the best of our knowledge, this study is the first to demonstrate an NDMA assay implemented on a paper-based microfluidic platform and is the first study to integrate the photochemical nitrosation reaction directly on-chip, which enables a complete photochemical–colorimetric workflow. By leveraging microfluidic technology, this approach broadens detection capabilities and paves the way for rapid, portable NDMA screening on fast-flow paper-based systems suitable for field deployment by non-experts.

2. Materials and methods

2.1. Chemicals and materials

NDMA was purchased from MilliporeSigma (Burlington, MA, USA). Sodium 1-naphthol-4-sulfonate, iron(II) chloride, and cobalt(II) sulfate heptahydrate were obtained from Fisher Scientific (Pittsburgh, PA, USA). Materials used for fabrication of the capillary flow-driven device included 468MP double-sided adhesive (DSA) and 9984 PET transparency film, both supplied by 3M Company (St. Paul, MN, USA). All aqueous solutions were prepared using Milli-Q water (18.2 MΩ cm). UV LED strips were purchased from Amazon (Seattle, WA, USA). Device components were patterned and cut using a CO_2 laser cutter (Epilog Zing; Golden, CO, USA). The UV irradiation chambers were fabricated using a fused deposition modeling (FDM) 3D printer (Bambu Lab P1S; Bambu Lab USA Inc., Austin, TX, USA).

2.2. Device fabrication

The capillary-driven microfluidic device consists of three inlets, three microfluidic channels, and three outlets, as illustrated in Fig. 1. The device is constructed as a three-layer

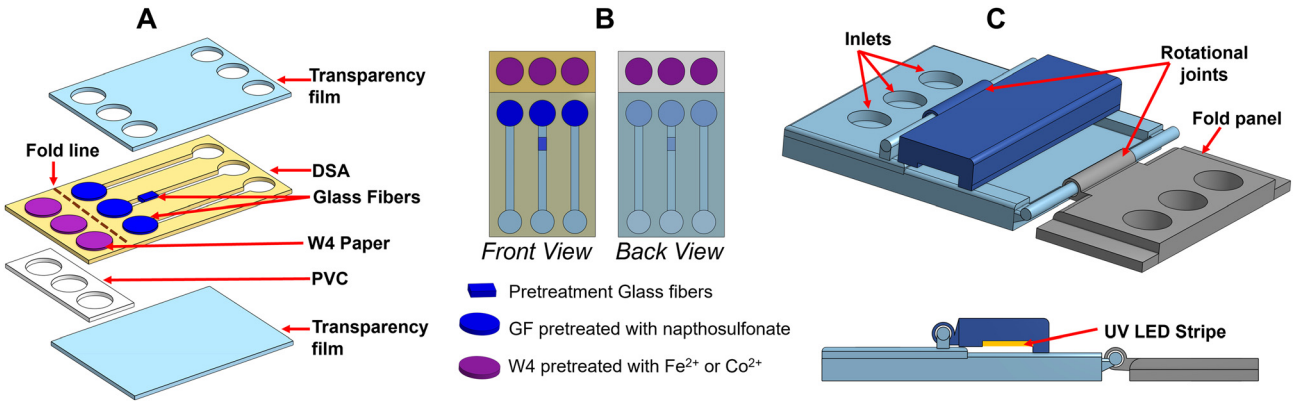

Fig. 1 Design and assembly of the capillary-driven microfluidic NDMA sensor and UV irradiation cassette. (A) Exploded view of the three-layer laminated microfluidic device showing patterned PET and double-sided adhesive layers, reagent-loaded glass fiber and paper pads, masking zone, and fold-over detection region. (B) Top and rear views of the assembled sensor illustrating inlet/detection zone alignment and channel layout. (C) Isometric (top) and side views of the 3D-printed UV cassette, highlighting the sensor-insertion module, UV LED irradiation hinge, and folding panel.

laminate composed of alternating sheets of 9984 PET transparency film and double-sided adhesive (Fig. 1A). Device layers were patterned using a CO_2 laser to define the microchannels, inlets, outlets, and reagent zones.[39–42] The detection zone is located at the bottom layer of the device and is folded over the outlet region during operation. During assembly, circular glass fiber pads (6 mm diameter) and Whatman Grade 4 filter paper discs (6 mm diameter) were cut and placed into designated regions of the device for reagent pretreatment, as shown in Fig. 1A. Sodium 1-naphthol-4-sulfonate (20 μL) was deposited and dried onto each glass fiber pad. Fe^{2+}; 5 μL and Co^{2+}; 5 μL solutions were deposited and dried onto the paper discs in channels 2 and 3, respectively. Additionally, after drying 1-naphthol-4-sulfonate on the third glass fiber pad, 10 μL of Co^{2+} solution was added and dried on the same pad. A glass fiber (2.5 mm × 5 mm) dried with 0.1 M NaF was placed in the middle of the second flowchannel as a masking zone. A polyvinyl chloride (PVC) backing was added beneath the detection zone to facilitate image acquisition by providing a uniform, non-reflective background. The fully assembled device measures 6 cm × 4 cm and is reduced to 4 cm × 4 cm after folding along the indicated line. Each microfluidic channel measures 18 mm × 2.5 mm (Fig. 1B). Channel 1 serves as a control, while channels 2 and 3 are designated for NDMA detection using Fe^{2+} and Co^{2+}, respectively.

A 3D-printed on-chip holder was developed to facilitate the photonitrosation reaction between NDMA and sodium 1-naphthol-4-sulfonate. The device was fabricated using polylactic acid (PLA) filament *via* fused deposition modeling (FDM) 3D printing. The design consists of three integrated components: (1) a microfluidic sensor-insertion module, (2) a UV irradiation hinge, and (3) a folding panel (Fig. 1C). The sensor-insertion module is designed to securely hold the disposable capillary-driven microfluidic sensor in a fixed position. At the distal end of this module, three inlet ports are aligned to correspond precisely with the three inlets of the microfluidic device, ensuring consistent sample introduction. The UV irradiation hinge incorporates a UV LED strip connected to an external power source. The hinge is positioned such that, when closed, the UV LEDs are aligned directly above the glass fiber reaction zones of the microfluidic sensor, enabling uniform and reproducible UV exposure during the photonitrosation reaction. The folding panel contains three circular apertures (9 mm diameter) that, upon folding, apply constant and uniform pressure across the reaction zones. This controlled folding ensures consistent contact between the metal-ion-impregnated paper pads and the photonitrosation complex formed on the glass fiber, thereby improving the reproducibility of color signal generation. The UV source consisted of a 365 nm LED strip operated with a constant 12 V power supply. The exposure time was optimized during method development (Fig. 3C), with 20 min selected as the optimal irradiation time based on signal saturation. The cassette design maintains a fixed distance and alignment between the LED strip and reaction zones, ensuring consistent and uniform irradiation across experiments. The UV cassette functions solely as a structural support and irradiation holder and does not come into direct contact with the fluidic channels. All reagents and samples are confined within the disposable device, minimizing the risk of cross-contamination.

2.3. Image analysis

Images of the paper pads on the microfluidic device were captured using a smartphone camera under controlled lighting conditions. Image analysis was performed using ImageJ software (NIH, USA). Each image was first separated into its red, green, and blue (RGB) color channels.[40] The blue channel was used for NDMA–Fe^{2+} analysis while the green channel was selected for NDMA–Co^{2+} analysis, as these channels exhibited the highest sensitivity for the respective assays (see Fig. S1). To minimize background interference,

the selected color channel image was inverted before analysis. A circular region of interest (ROI) was defined over each paper pad, and the mean grayscale intensity was calculated. For each device, intensity values were averaged across three ROIs corresponding to the three flow channels. Measurements obtained for the same NDMA concentration were further averaged. Unless otherwise stated, all experiments were performed in triplicate using three parallel channels within a single capillary flow-driven device, and method validation was conducted using three independent devices, each incorporating a control channel along with one Fe^{2+}-based detection channel, and one Co^{2+}-based detection channel. This standardized image acquisition and processing workflow was effective during assay development and laboratory validation. For on-site or field-based applications, a simplified analysis protocol may be employed, such as the use of a color reference chart or a uniform white background to normalize lighting variations.[43–45] In addition, the compatibility of the rapid-flow sensor with the RGB Color Detector—a readily available mobile image-analysis smartphone application—was demonstrated, enabling portable and on-site quantitative analysis when required (Fig. S2).

2.4. Assay principle

The proposed mechanism for the on-chip colorimetric reactions illustrated in Fig. 2 is adapted from a previously reported study.[38] Under UV irradiation, NDMA undergoes photolysis to generate nitrosating species that react with the photoacidic sodium 1,4-naphtholsulfonate, resulting in a photonitrosation that converts the naphthol into an *ortho*-naphthoquinone-oxime *via* a naphthol-as-acid excited-state proton transfer mechanism analogous to Chow's naphthol nitrosation chemistry.[46] The quinone-oxime product on its own is only weakly colored, but its oxime N/O donors and adjacent quinone O atoms form a strong chelating ligand for Fe(II) and Co(II); mixing the *ortho*-naphthoquinone-oxime with Fe(II) or Co(II) in near-neutral aqueous solution produces a tris-chelate Fe(II) or Co(II) complex, respectively (Fig. 2).[38] The tris-chelate Fe(II) complex is green, whereas the tris-chelate Co(II) complex is red.

3. Results and discussion

3.1. Sensor performance

The performance of the capillary-driven microfluidic sensor was evaluated in terms of user-friendliness, multiplexing capability, flow rate, reaction time, time required for color formation, and homogeneity of the colorimetric complex. A key challenge in NDMA detection using the photochemical method is performing multiple chemical reactions on a single chip while preventing reagents from reacting prematurely and ensuring they are available when needed. This was addressed through an on-chip design that uses lateral flow, allowing reagents to be separated within hollow channels and stored without interacting until the test is performed. Moreover, the device is designed so that capillary flow transports the analyte sample upon dipping, enabling rapid flow while minimizing analyte loss due to adsorption, a common limitation of conventional paper-based microfluidic systems.[27,47] The controlled delivery of sample volume is governed by the geometry of the hollow capillary channels. The channel dimensions (length, width, and height) are precisely defined through laser cutting, resulting in a fixed internal volume. Upon dipping, capillary action fills the channel until it is completely occupied, at which point flow naturally stops as shown in Movie S1. This self-limiting mechanism ensures consistent and reproducible sample volumes without the need for external volume control or precise pipetting, which is advantageous for field applications. Another challenge was enabling UV irradiation on-chip, as most miniaturized systems focus on colorimetry, electrochemistry, or qualitative readouts. In this system, the photochemical reaction is followed by colorimetric detection, so incorporating a UV source directly into the hollow channels was not feasible. To address this, a reusable 3D-printed cassette was designed to perform photonitrosation

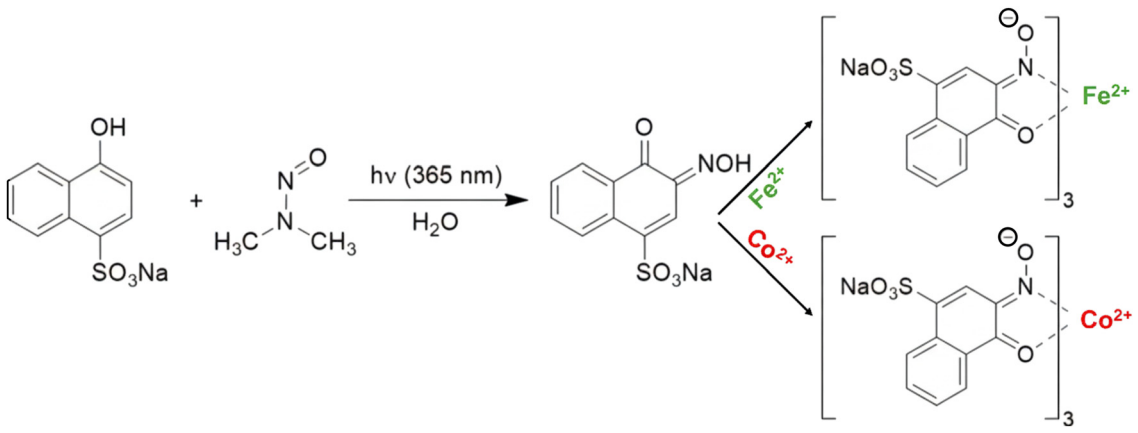

Fig. 2 Proposed chromogenic reaction mechanism of NDMA with 1-naphthol-4-sulfonate and Fe^{2+} or Co^{2+}. Adapted from ref. 38.

easily. The cassette is inexpensive, user-friendly, portable, and can be reused, allowing the UV step to be carried out on-site.

The microfluidic device's channel geometry was optimized for fast and consistent flow, with a width of 2.5 mm, a detection zone diameter of 6 mm, a sample inlet diameter of 6 mm, and a channel height of 350 μm (see Fig. S3 and S4). The channel dimensions were designed to achieve consistent capillary flow rates and complete saturation of the glass fiber detection pads within a defined time frame. Ensuring full and uniform saturation of the pads is critical for consistent reagent interaction and signal development. Additionally, the geometry was optimized to maintain comparable flow behavior across multiple channels, enabling uniform sample delivery and reproducible assay performance. These results are consistent with the optimal channel geometries we have achieved in our previous studies.[40,44]

Whatman Grade 1, Whatman Grade 3, Whatman Grade 4, and Ahlstrom blotting paper 319 were evaluated for signal intensity and response homogeneity (see Fig. S5). Whatman Grade 4 provided the most uniform and reproducible signal and was selected for all subsequent experiments. The improved signal consistency observed with Whatman Grade 4 paper is attributed to its larger pore size and higher permeability, which facilitates faster and more uniform capillary flow.[48] These properties enable efficient reagent transport and homogeneous distribution within the detection zone, ensuring consistent saturation and reproducible color development.

Naphthosulfonate pads were primarily composed of glass microfiber to ensure rapid release of immobilized reagents due to their high surface chemistry. Technical specifications for different substrates tested in this study are provided in Table S1. The concentration of sodium 1-naphthol-4-sulfonate was optimized by evaluating concentrations of 0.25, 0.5, 1.0, 1.5, and 2.0 mg mL^{-1} (Fig. 3A). Signal intensity increased with concentration up to 0.5 mg mL^{-1}, beyond which no significant improvement was observed. This plateau suggests that the reaction reaches a saturation regime, where sufficient reagent is available for complete reaction. At higher concentrations, increased background signals and reduced contrast were observed. Therefore, 0.5 mg mL^{-1} was selected as the optimal concentration. Reaction time was optimized for both Fe^{2+}- and Co^{2+}-based detection by monitoring signal development from 1 to 15 min (Fig. 3B). The color intensity increased rapidly within the first 5 min and showed no statistically significant enhancement thereafter; thus, 5 min was chosen as the optimal imaging time. UV irradiation time was optimized by testing exposure durations of 5, 10, 15, 20, 25, and 30 min (Fig. 3C). Signal intensity increased up to 20 min and then reached a plateau, indicating completion of the photonitrosation reaction; therefore, 20 min was selected. Finally, the concentrations of metal salts immobilized on the paper pads were optimized

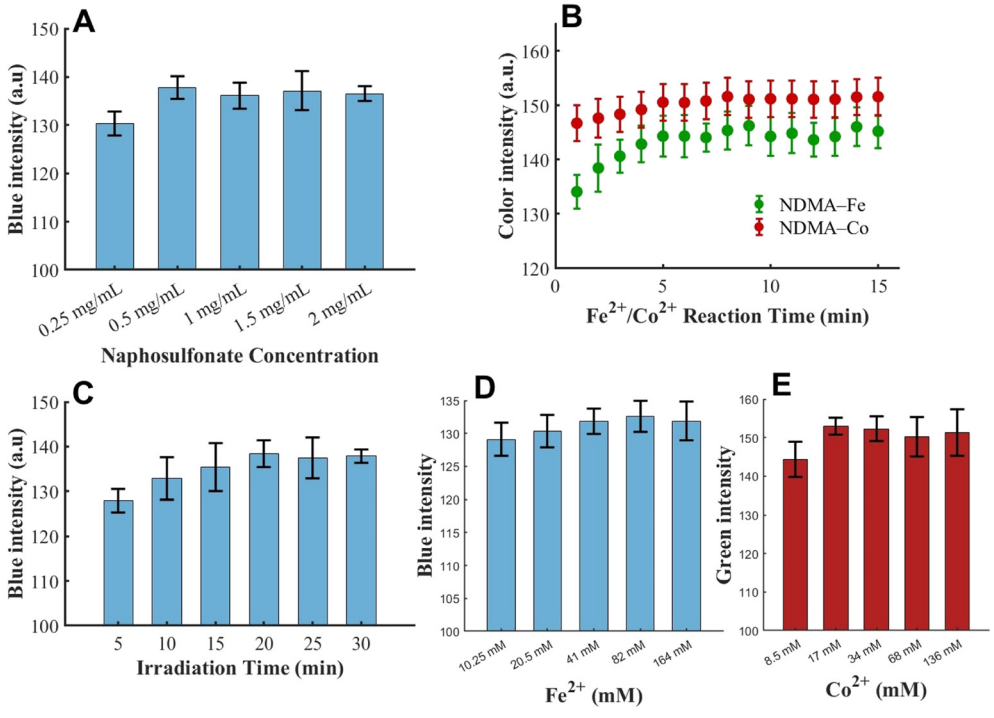

Fig. 3 Optimization of assay parameters for paper-based NDMA detection. (A) Effect of sodium 1-naphthol-4-sulfonate concentration on color intensity, with 0.5 mg mL^{-1} selected as the optimal concentration. (B) Optimization of reaction time for Fe^{2+}- and Co^{2+}-based assays, showing signal saturation at 5 min. (C) Effect of UV irradiation time on signal development, with a plateau observed at 20 min, indicating completion of the photonitrosation reaction. (D) Optimization of Fe^{2+} concentration and (E) optimization of Co^{2+} concentration on the paper pads to maximize signal intensity while minimizing variability.

by evaluating Fe^{2+} concentrations of 10.25, 20.5, 41, 82, and 164 mM and Co^{2+} concentrations of 8.5, 17, 34, 68, and 136 mM (Fig. 3D and E). Optimal signal intensity with minimal variation was obtained at 41 mM Fe^{2+} and 17 mM Co^{2+}, which were used for all subsequent measurements. No further improvements were observed at higher concentrations.

In our previous work on capillary flow-driven microfluidic systems, temperature and humidity were shown to have no significant effect on flow behavior under typical conditions.[44] The device is designed for aqueous samples where viscosity variations are minimal; moreover, during interference studies involving surfactants, no observable changes in flow behavior were noted despite their potential to alter fluid properties. Overall, the enclosed channel design and capillary-driven architecture ensure consistent and reproducible flow under realistic operating conditions. In real field deployment scenarios, variability arising from inconsistent lighting conditions can be mitigated using internal reference and control zones. This normalization approach also compensates for potential sample coloration effects, enabling more reliable quantitative analysis, as shown in eqn (1).[49]

$$\text{Relative Intensity} = \frac{I(\text{reaction zone}) - I(\text{control zone})}{I(\text{reference zone})} \quad (1)$$

3.2. Calibration and analytical figures of merit

Calibration curves for the NDMA–Fe^{2+} and NDMA–Co^{2+} assays were constructed by plotting color intensity as a function of NDMA concentration (Fig. 4). For the NDMA–Fe^{2+}-based detection system, calibration was performed over a concentration range of 0–150 ppm, with a linear response observed from 0–100 ppm (Fig. 4A). Similarly, the NDMA–Co^{2+} system was calibrated over a range of 0–100 ppm but exhibited a lower linear dynamic range of 0–30 ppm (Fig. 4B). Beyond the respective linear ranges, little to no additional increase in color intensity was observed, as the paper-based detection zones reached maximum color saturation and the signal plateaued. The linear equations for the systems were determined as $y = (0.47 \pm 0.03)x + (116.60 \pm 1.73)$ for the NDMA–Fe^{2+} system and $y = (1.95 \pm 0.09)x + (101.10 \pm 1.32)$ for the NDMA–Co^{2+} system. The limits of detection (LoD) and quantification (LoQ) were determined to be 4 ppm and 14 ppm for the NDMA–Fe^{2+} system, and 1.5 ppm and 5 ppm for the NDMA–Co^{2+} system, respectively. The LoD was calculated as three times the standard deviation (SD) of the blank divided by the slope of the calibration curve, while the LoQ was calculated as ten times the SD of the blank divided by the slope (n = 9).[50] The sensitivity was calculated to be 0.47 ± 0.03 a.u. ppm^{-1} for the NDMA–Fe^{2+} system and 1.95 ± 0.09 a.u. ppm^{-1} for the NDMA–Co^{2+} system. Although the LoD values reported here are higher than NDMA concentrations typically found in drinking water, most regulatory detection methods, such as GC-MS or LC-HRMS incur their major costs from the need for sophisticated instrumentation, specialized columns, and highly trained personnel. Therefore, when existing preconcentration approaches are integrated with this portable paper-based sensor, the platform offers a cost-effective and field-deployable alternative that maintains analytical reliability for high-frequency, on-site NDMA monitoring. To the best of our knowledge, this represents the first μPAD based lab-on-a-chip platform for NDMA detection, an emerging contaminant of increasing environmental concern.

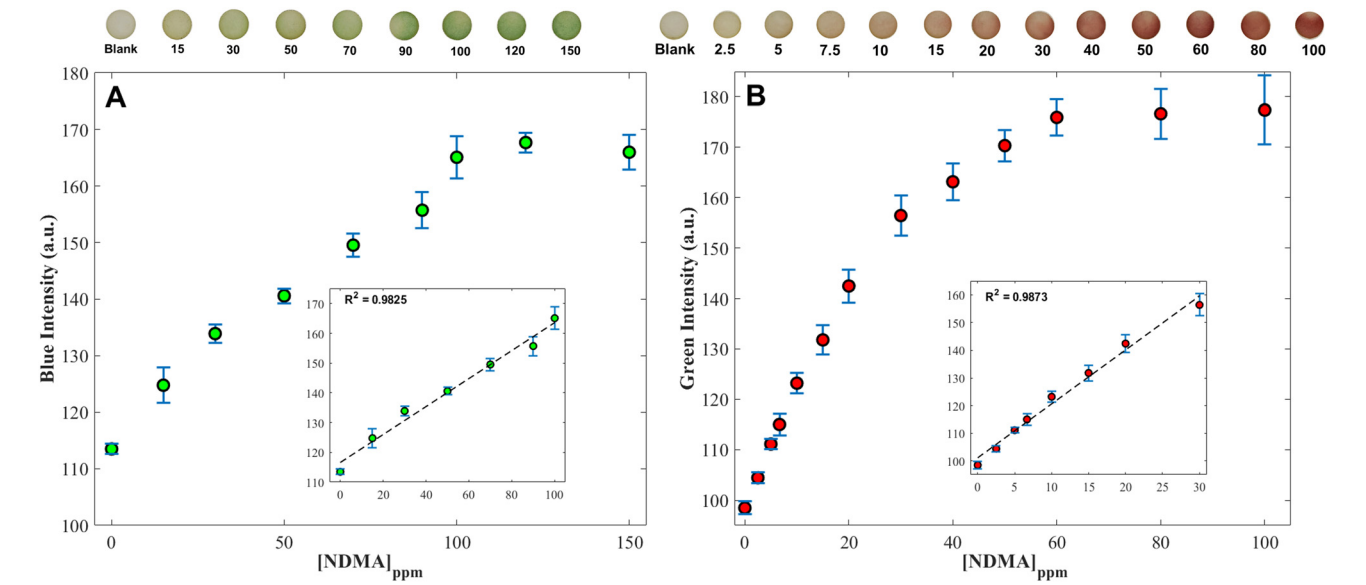

Fig. 4 Calibration curves for NDMA detection using (A) NDMA–Fe^{2+} and (B) NDMA–Co^{2+} paper-based assays. Color intensity is plotted as a function of NDMA concentration. Insets show the corresponding linear response regions used for calibration analysis. The NDMA–Fe^{2+} system exhibited a linear response from 0–100 ppm, while the NDMA–Co^{2+} system showed a linear dynamic range from 0–30 ppm. Error bars represent ± SD (n = 3).

Moreover, unlike other reported sensing systems, the capillary flow-driven devices presented here are inherently disposable, simple to operate, and require minimal external hardware. The reagents are strategically separated within the detection zones to prevent cross-reactivity, enhancing the device's long-term stability.[44] Each sensor is designed for single use, and the 3D printed cassette is reusable without any maintenance, therefore there is no need for regular maintenance or calibration. Furthermore, unlike electrochemical sensors, the developed platform operates reliably without the need for sample stirring. To further improve its user-friendliness, the colorimetric signal could be processed using a custom-developed or commercially available smartphone application instead of ImageJ. Previous studies support the effectiveness of quantifying colorimetric signals in fast-flow microfluidic devices.[43,44] For field calibration, we have previously demonstrated the use of smartphone-based tools, such as RGB Color Detector and MATLAB Mobile, which enable on-site calibration and quantification using standard solutions or reference color charts.[44,51] These approaches allow practical and accessible calibration under field conditions. The reproducibility of the photochemical reaction under deployment conditions is ensured by the standardized design of the UV cassette and simplified operation. The system requires only two user steps (dip and fold), with the folding process controlled by the cassette to maintain consistent alignment and contact. In addition, the use of a fixed UV source, constant operating conditions, and defined exposure time ensures reproducible irradiation and reaction conditions across measurements.

3.3. Interference study

To evaluate potential interference in the NDMA assays, interference studies were conducted for both the NDMA–Fe^{2+} and NDMA–Co^{2+} systems at a 1 : 1 ratio of NDMA to potential interferents (Fig. 5A and B, respectively). The following ions and species were examined: Fe^{3+}, Li^{+}, Na^{+}, Pb^{+}, Ag^{+}, Mg^{2+}, Ca^{2+}, Ba^{2+}, Zn^{2+}, Cd^{2+}, SO_4^{2-}, PO_4^{3-}, HCO_3^{-}, Co^{2+}, Ni^{2+}, and Cu^{2+}, along with two representative surfactants (Surf 1: sodium dodecyl sulfate, Surf 2: tetramethyl(tetradecyl) ammonium chloride). In the bar plots, green bars represent the control (NDMA only) for the respective reactions, blue bars represent responses from NDMA mixed with potential interferents showing no significant interference, and red bars indicate significant interference. For the NDMA–Fe-based system, significant interference was observed from Cu^{2+} and Co^{2+}. NaF was incorporated as a masking agent to selectively complex interfering metal ions, particularly Cu^{2+}, thereby preventing undesired interactions with the nitrosated chromophore and improving the selectivity of the Fe^{2+}-based detection channel.[40,51] This strategy is based on our prior

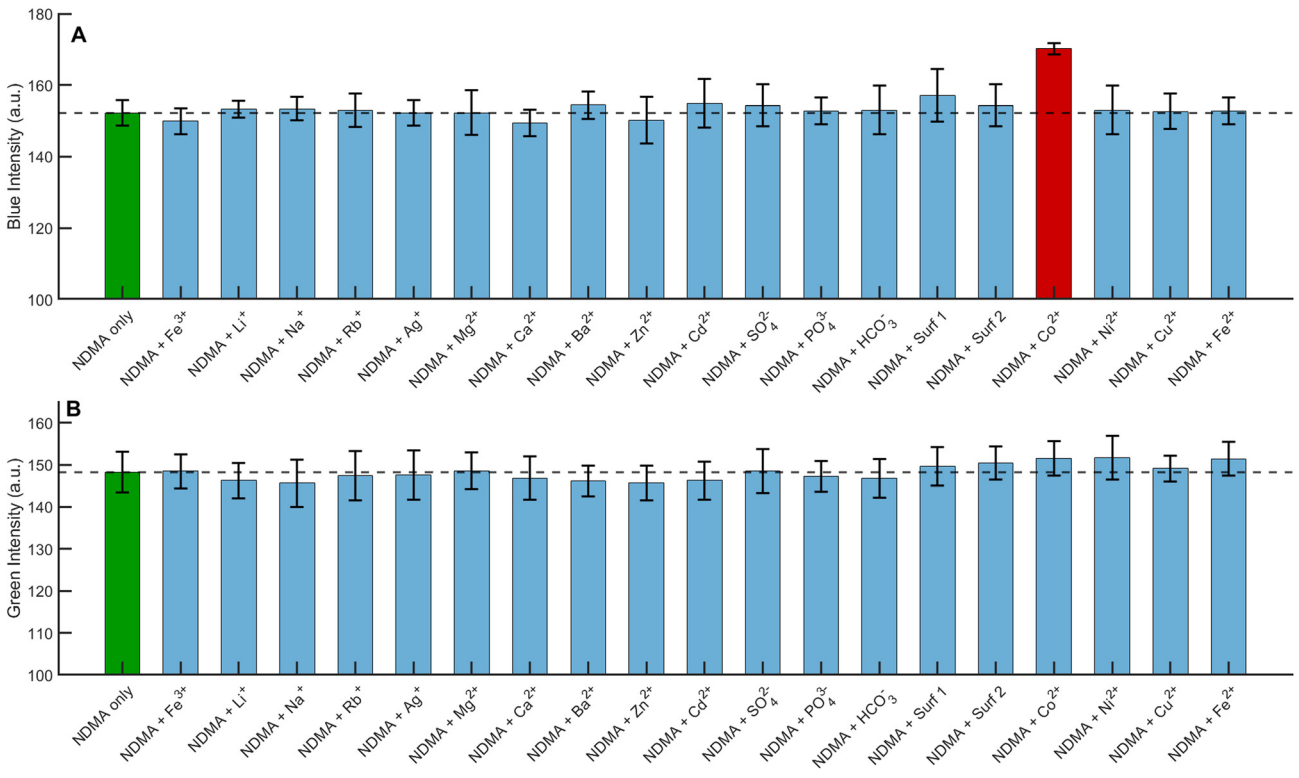

Fig. 5 Interference studies for NDMA detection using (A) NDMA–Fe^{2+} and (B) NDMA–Co^{2+} paper-based assays. Assays were performed at a 1 : 1 ratio of NDMA to potential interferents. Green bars represent the NDMA-only control, blue bars indicate NDMA in the presence of potential interferents showing no significant interference, and red bars denote significant interference. Significances were tested using Dunnett's multiple comparison test (α = 0.05).

work on screening and identifying effective masking agents and has since been adopted in related studies.[40,51,52] In contrast, interference from Co^{2+} could not be effectively masked using reported methods in the literature without compromising assay sensitivity. In the presence of Co^{2+}, the color response changed from green to red. However, this does not pose a practical limitation because in water samples containing substantial Co^{2+} levels, detection can instead rely on the NDMA–Co^{2+} system, for which no significant interference was observed (Fig. 5B). Notably, the color signal produced by the NDMA–Co^{2+} system was sufficiently strong to overshadow any potential interference from Cu^{2+} or Fe^{2+}. The use of two detection systems with distinct dynamic ranges, therefore, provides a complementary, hybrid sensing strategy. Although a previous solution-based study reported faint color development from Ni^{2+} in the NDMA–naphthosulfonate assay, no significant interference from Ni^{2+} was observed in either of the paper-based assays.[38] This is likely due to suppression of the weak Ni^{2+}-related signal by the much stronger color responses associated with Fe^{2+} or Co^{2+} on the paper platform, consistent with the very faint color formation reported in solution.[38]

3.4. Stability and sustainability

The stability of Fe^{2+}-based (Fig. 6A) and Co^{2+}-based (Fig. 6B) NDMA sensors was assessed under three storage conditions: room temperature (RT), refrigeration (5 °C), and freezing (−20 °C). Devices were stored in black Mylar bags containing activated molecular sieves, purged with nitrogen, and vacuum sealed. Sensor performance was evaluated over four weeks. Under refrigerated (5 °C) and frozen (−20 °C) storage, both sensor types maintained signal intensities comparable to day-0 values throughout the study period. In contrast, sensors stored at room temperature lost ~10% of their initial signal over four weeks, with measurable signal degradation observed after the first week. These results indicate that the devices can be batch-manufactured, shipped, and stored for practical field deployment without significant loss of performance. Additionally, the environmental sustainability of the sensor was assessed using the Analytical GREEnness (AGREE) metric, which evaluates adherence to 12 principles of green analytical chemistry, including minimization of reagent consumption and waste, reduction of toxic reagent usage, and ensuring operator safety.[53] As shown in Fig. S6, the sensor achieved a greenness score of 0.83, placing it firmly within the "greener" zone and demonstrating its environmentally friendly design. The AGREE assessment highlights the alignment of the developed platform with green analytical chemistry principles, including minimal sample and reagent consumption, low energy requirements, and integration of sampling, reaction, and detection into a single device. These attributes reduce waste generation, minimize user exposure, and eliminate extensive sample preparation, underscoring the platform's potential as a sustainable solution for field-based environmental monitoring (see Table S1).

3.5. Analysis of real water samples

To evaluate the sensor's performance in complex matrices, surface water samples were collected from campus tap water, the Cache La Poudre River, and Sheldon Lake (GPS coordinates: 40°35′42.2″N 105°04′32.5″W, and 40°34′56.7″N 105°06′09.9″W, respectively). Since the natural concentrations of the target analyte were below the sensor's detection limits, spike recovery experiments were performed as an analytical validation method.[54] Three concentrations of NDMA were spiked into each sample, selected to exceed the sensor's limit of detection (LoD) while remaining below saturation levels. For the NDMA–Fe^{2+}-based system, NDMA was spiked at concentrations of 25, 50, and 75 ppm. The spike recovery experiments were performed in triplicate (n = 3) for each concentration level and water matrix using three independent devices. Recovery values and %RSD were calculated as the mean and relative standard deviation of these measurements. In tap water, recoveries ranged from 93–95% with relative standard deviations (RSDs) of 7.8–9.5%. River water samples showed recoveries of 81–83% with RSDs between 6.6 and 9.9%, while lake water samples exhibited recoveries of 76–81% with RSDs of 5.7–9.0% (Table 1). The analytical

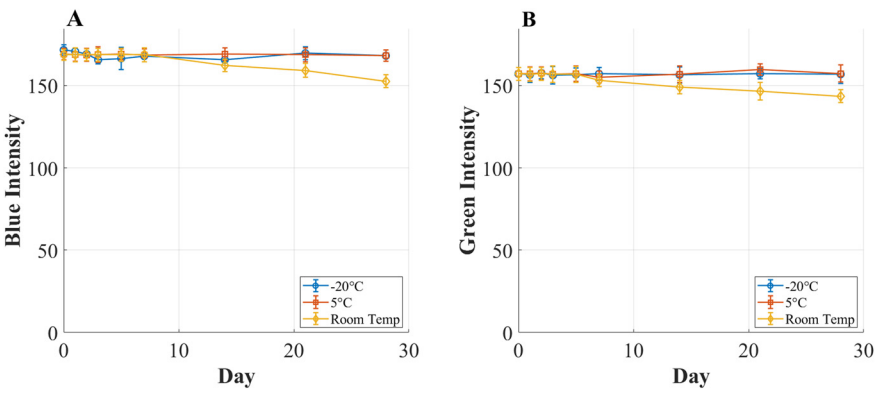

Fig. 6 Stability of NDMA sensors under different storage conditions. Stability of (A) Co^{2+}-based and (B) Fe^{2+}-based NDMA sensors stored at room temperature, 5 °C, and −20 °C, with signal intensity monitored over four weeks.

Table 1 Spike recovery results for NDMA in real-water samples using the NDMA–Fe^{2+}-based detection system

Water type	Spiked (ppm)	Recovered (ppm)	%Recovery	%RSD
Tap water	0	ND	—	—
	25	23.3 ± 2.2	93	9.5
	50	47.2 ± 3.7	94	7.8
	75	71.3 ± 6.5	95	9.2
River water	0	ND	—	—
	25	20.4 ± 2.0	81	9.9
	50	41.3 ± 3.6	83	8.8
	75	62.6 ± 4.2	83	6.6
Lake water	0	ND	—	—
	25	19.6 ± 1.8	78	9.0
	50	40.7 ± 2.3	81	5.7
	75	56.9 ± 4.5	76	7.9

performance of the NDMA–Co^{2+}-based sensor was similarly assessed by spiking NDMA at 5, 15, and 25 ppm to evaluate sensor performance at lower concentration levels (n = 3). In tap water, recoveries ranged from 95–98% with RSDs of 6.1–7.4%. River water samples yielded recoveries of 81–86% with RSDs between 5.9 and 7.3%, while lake water samples showed recoveries of 76–80% with RSDs of 7.5–9.4% (Table 2). As expected, the inter-device variation is higher than the intra-device variation (as shown in Table S3), due to additional sources of variability associated with independent device fabrication and matrix effects present in real water samples. Nevertheless, the recovery values within each specific water type were highly consistent across the tested concentration levels, typically varying within a narrow range (≈5%), with RSD < 10%. The observed %RSD values (<10%) indicate acceptable precision for field-deployable analytical methods and are consistent with commonly accepted criteria for environmental analysis. According to standard method validation guidelines, RSD values below 10–15% are generally considered acceptable for complex environmental samples, particularly for portable and screening-level techniques.[54] In addition to quantitative analysis, the platform can function as a semi-quantitative or qualitative screening tool, analogous to widely used field tests such as pH strips, nitrate/nitrite kits, and chlorine test strips, where approximate concentration ranges are sufficient for decision-making.

Table 2 Spike recovery results for NDMA in real-water samples using the NDMA–Co^{2+}–based detection system

Water type	Spiked (ppm)	Recovered (ppm)	%Recovery	%RSD
Tap water	0	ND	—	—
	5	4.9 ± 0.3	98	6.1
	15	14.2 ± 1.1	95	7.4
	25	23.8 ± 1.6	95	6.9
River water	0	ND	—	—
	5	4.3 ± 0.3	86	6.4
	15	12.3 ± 0.7	82	5.9
	25	20.4 ± 1.5	81	7.3
Lake water	0	ND	—	—
	5	3.8 ± 0.3	76	8.0
	15	11.6 ± 0.9	77	7.5
	25	20.0 ± 1.9	80	9.4

4. Conclusion

In summary, we present, to the best of our knowledge, the first lab-on-a-chip platform for NDMA detection and the first system integrating on-chip photochemical nitrosation and colorimetric detection within a single workflow. This platform enables rapid, portable, and user-friendly analysis, representing a significant step toward translating traditional laboratory-based NDMA detection methods into field-deployable formats. A key challenge in NDMA detection using photochemical methods is performing multiple reactions on a single chip without premature reagent mixing. This was addressed using lateral-flow channels that store reagents separately and allow controlled analyte transport upon dipping, minimizing loss and eliminating the need for pipetting. Another challenge was enabling UV irradiation for the photochemical reaction, which cannot be integrated directly into the channels. This was solved with a reusable, portable 3D-printed cassette that performs photonitrosation easily and cost-effectively, followed by colorimetric detection on the chip. The sensor operates in two simple steps: dip and fold—without the need for pipetting or specialized instruments for readout. The device achieves detection limits of 1.5 ppm and 4 ppm for Co^{2+}- and Fe^{2+}-based sensors, respectively, with complementary linear ranges extending to 30 ppm and 100 ppm. Dual-channel multiplexing combined with a proper masking strategy provides higher selectivity in real sample matrices. The assay is completed in under 25 minutes, exhibits excellent storage stability, and demonstrates high analytical reliability with RSD < 10% in real water samples. With a high greenness score (0.83, AGREE metrics), low device cost (<$0.20), and straightforward smartphone-based readout, this platform offers a portable, user-friendly, and sustainable alternative to conventional lab-based methods such as GC-MS/MS, enabling decentralized, high-frequency NDMA monitoring. While the current detection limits are in the ppm range, we acknowledge that achieving environmentally relevant sensitivity will require the integration of preconcentration strategies. Ongoing work in our group is focused on developing preconcentration modules, including the evaluation of capture efficiencies of various filter materials, to be coupled with this platform. These efforts are expected to further enhance the analytical performance and broaden the applicability of the system for trace-level environmental monitoring. Furthermore, the approach is adaptable for other on-chip photochemical reactions in paper-based and other microfluidic systems that can be used to detect a wide variety of further contaminants.

Author contributions

Prakash Aryal: conceptualization, methodology, investigation, writing – original draft, writing – review & editing. Jade Manna-Rubenstein: investigation, writing – review & editing. Tessa Whitaker: investigation, writing – review & editing. Eric

Brack: conceptualization, supervision, funding acquisition, writing – review & editing. Charles S. Henry: conceptualization, supervision, funding acquisition, writing – review & editing.

Conflicts of interest

The authors declare no known competing financial interests or personal relationships that could have influenced the work reported in this paper.

Data availability

The data supporting the findings of this study are available from the corresponding author upon reasonable request.

Supplementary information (SI) is available. See DOI: https://doi.org/10.1039/d6lc00165c.

Acknowledgements

The authors would like to acknowledge the financial support provided for this project by the US Army DEVCOM Center Natick, MA through contract W911QY2120003. PA would also like to acknowledge the financial support from the American Chemical Society Analytical Graduate Research Fellowship. This work has been reviewed and approved for public release under OPSEC Form ID 3039, Approval Number PR2026-3039.

References

1 W. A. Mitch, J. O. Sharp, R. R. Trussell, R. L. Valentine, L. Alvarez-Cohen and D. L. Sedlak, *N*-Nitrosodimethylamine (NDMA) as a Drinking Water Contaminant: A Review, *Environ. Eng. Sci.*, 2003, **20**(5), 389–404, DOI: 10.1089/109287503768335896.

2 Syracuse Research Corporation, Clement Associates, *Toxicological profile for N-nitrosodimethylamine*, Agency for Toxic Substances and Disease Registry, 1989.

3 N. Van Huy, M. Murakami, H. Sakai, K. Oguma, K. Kosaka and M. Asami, *et al.*, Occeurrence and formation potential of *N*-nitrosodimethylamine in ground water and river water in Tokyo, *Water Res.*, 2011, **45**(11), 3369–3377, DOI: 10.1016/j.watres.2011.03.053.

4 C. D. Water, Guidelines for Canadian drinking water quality, In: *Summary table*, 2021, Available from: https://www.canada.ca/en/health-canada/services/environmental-workplace-health/reports-publications/water-quality/guidelines-canadian-drinking-water-quality-summary-table.html.

5 A. Ray, S. Atal and B. Sadasivam, Understanding the molecular–pharmaceutical basis of sartan recalls focusing on valsartan, *Glob. Cardiol. Sci. Pract.*, 2020, **2020**(2), e202025.

6 J. C. Beard and T. M. Swager, An Organic Chemist's Guide to *N*-Nitrosamines: Their Structure, Reactivity, and Role as Contaminants, *J. Org. Chem.*, 2021, **86**(3), 2037–2057, DOI: 10.1021/acs.joc.0c02774.

7 USEPA, Technical fact sheet–N-nitroso-dimethylamine (NDMA), In: https://www.epa.gov/sites/default/files/2017-10/documents/ndma_fact_sheet_update_9-15-17_508.pdf, 2014.

8 G. Abulikemu, J. H. Mistry, D. G. Wahman, M. T. Alexander, A. R. Kennicutt and J. D. Bollman, *et al.*, Investigation of Chloramines, Disinfection Byproducts, and Nitrification in Chloraminated Drinking Water Distribution Systems, *J. Environ. Eng.*, 2022, **149**(1), 1–12, DOI: 10.1061/(asce)ee.1943-7870.0002062, PubMed PMID: 37593338; PubMed Central PMCID: PMC10430769.

9 C. J. Seidel, M. J. McGuire, R. S. Summers and S. Via, Have utilities switched to chloramines?, *J. Am. Water Works Assoc.*, 2005, **97**, 87–97, DOI: 10.1002/j.1551-8833.2005.tb07497.x.

10 H. T. Pham, D. G. Wahman and J. L. Fairey, Updated reaction pathway for dichloramine decomposition: Formation of reactive nitrogen species and N-nitrosodimethylamine, *Environ. Sci. Technol.*, 2021, **55**(3), 1740–1749, DOI: 10.1021/acs.est.0c06456.

11 Y. D. Liu, M. Selbes, C. Zeng, R. Zhong and T. Karanfil, Formation Mechanism of NDMA from Ranitidine, Trimethylamine, and Other Tertiary Amines during Chloramination: A Computational Study, *Environ. Sci. Technol.*, 2014, **48**(15), 8653–8663, DOI: 10.1021/es500997e, PubMed PMID: 24968236; PubMed Central PMCID: PMC4123930.

12 J. Choi and R. L. Valentine, Formation of N-nitrosodimethylamine (NDMA) from reaction of monochloramine: a new disinfection by-product, *Water Res.*, 2002, **36**(4), 817–824, DOI: 10.1016/S0043-1354(01)00303-7.

13 S. Spahr, O. A. Cirpka, U. Von Gunten and T. B. Hofstetter, Formation of *N*-Nitrosodimethylamine during Chloramination of Secondary and Tertiary Amines: Role of Molecular Oxygen and Radical Intermediates, *Environ. Sci. Technol.*, 2017, **51**(1), 280–290, DOI: 10.1021/acs.est.6b04780.

14 Potential For Human Exposure, In: *Toxicological Profile for N-Nitrosodimethylamine (NDMA)*, Agency for Toxic Substances and Disease Registry (US), 2023, Available from: https://www.ncbi.nlm.nih.gov/books/NBK601154/.

15 W. A. Mitch, J. O. Sharp, R. R. Trussell, R. L. Valentine, L. Alvarez-Cohen and D. L. Sedlak, *N*-Nitrosodimethylamine (NDMA) as a Drinking Water Contaminant: A Review, *Environ. Eng. Sci.*, 2003, **20**(5), 389–404, DOI: 10.1089/109287503768335896.

16 U. S. Environmental Protection.Agency, Technical Fact Sheet – N-Nitroso-dimethylamine (NDMA), 2017, Report EPA 505-F-17-005, Available from: https://19january2021snapshot.epa.gov/sites/static/files/2017-10/documents/ndma_fact_sheet_update_9-15-17_508.pdf.

17 State Water Resources Control Board, Division of Drinking Water, Nitrosamines – Drinking Water Issues (NDMA), 2025, Available from: https://www.waterboards.ca.gov/drinking_water/certlic/drinkingwater/NDMA.html.

18 Agency for Toxic Substances and Disease Registry, *Toxicological Profile for N-Nitrosodimethylamine (NDMA)*, U.S. Department of Health and Human Services, Public Health Service, 2023, Available from: https://www.atsdr.cdc.gov/toxprofiles/tp141.pdf.

19 G. McGwin, The Association between Ranitidine Use and Gastrointestinal Cancers, *Cancers*, 2020, **13**(1), 24, DOI: 10.3390/cancers13010024, PubMed PMID: 33374592; PubMed Central PMCID: PMC7793066.

20 I. Mansouri, J. Botton, L. Semenzato, N. Haddy and M. Zureik, N-nitrosodimethylamine-Contaminated Valsartan and Risk of Cancer: A Nationwide Study of 1.4 Million Valsartan Users, *J. Am. Heart Assoc.*, 2022, **11**(24), e8067, DOI: 10.1161/JAHA.122.026739, PubMed PMID: 36533625; PubMed Central PMCID: PMC9798794.

21 A. Pottegård, K. B. Kristensen, M. T. Ernst, N. B. Johansen, P. Quartarolo and J. Hallas, Use of N-nitrosodimethylamine (NDMA) contaminated valsartan products and risk of cancer: Danish nationwide cohort study, *BMJ*, 2018, k3851, DOI: 10.1136/bmj.k3851.

22 A. Pottegård, K. B. Kristensen, M. T. Ernst, N. B. Johansen, P. Quartarolo and J. Hallas, Use of N-nitrosodimethylamine (NDMA) contaminated valsartan products and risk of cancer: Danish nationwide cohort study, *BMJ*, 2018, 362.

23 W. A. Mitch, J. O. Sharp, R. R. Trussell, R. L. Valentine, L. Alvarez-Cohen and D. L. Sedlak, N-nitrosodimethylamine (NDMA) as a drinking water contaminant: a review, *Environ. Eng. Sci.*, 2003, **20**(5), 389–404, DOI: 10.1089/109287503768335896.

24 A. Cordner, G. Goldenman, L. S. Birnbaum, P. Brown, M. F. Miller and R. Mueller, *et al.*, The true cost of PFAS and the benefits of acting now, *Environ. Sci. Technol.*, 2021, **55**(14), 9630–9633, DOI: 10.1021/acs.est.1c03565.

25 E. M. Bell, S. De Guise, J. R. McCutcheon, Y. Lei, M. Levin and B. Li, *et al.*, Exposure, health effects, sensing, and remediation of the emerging PFAS contaminants–Scientific challenges and potential research directions, *Sci. Total Environ.*, 2021, **780**, 146399, DOI: 10.1016/j.scitotenv.2021.146399.

26 S. Y. Wee and A. Z. Aris, Revisiting the "forever chemicals", PFOA and PFOS exposure in drinking water, *npj Clean Water*, 2023, **6**(1), 57, DOI: 10.1038/s41545-023-00274-6.

27 P. Aryal and C. S. Henry, Advancements and challenges in microfluidic paper-based analytical devices: design, manufacturing, sustainability, and field applications, *Front. Lab. Chip. Technol.*, 2024, **3**, 1467423, DOI: 10.3389/frlct.2024.1467423.

28 J. Munch and M. Bassett, *Method 521: Determination of nitrosamines in drinking water by solid phase extraction and capillary column gas chromatography with large volume injection and chemical ionization tandem mass spectrometry (MS/MS)*, National Exposure Research Laboratory, Office of Research and Development, U.S. Environmental Protection Agency, Cincinnati, Ohio, 2004.

29 EEA-Agilent Method 521.1 Inter-Laboratory Comparison Study Quality Control Summary Report, 2024, Available from: https://www.waterboards.ca.gov/drinking_water/certlic/drinkingwater/docs/2024/eea-agilent-521-1-qc-summary.pdf.

30 K. A. Schug, The University of Texas at Arlington and D. D. Carlton Jr., *Evaluation of Automated Solid-Phase Extraction for Nitrosamines Using US EPA Method 521*, LCGC Supplements, 2016, vol. 13, issue 3.

31 F. Breider and U. von Gunten, Quantification of total N-nitrosamine concentrations in aqueous samples via UV-photolysis and chemiluminescence detection of nitric oxide, *Anal. Chem.*, 2017, **89**(3), 1574–1582, DOI: 10.1021/acs.analchem.6b03595.

32 A. D. Ngongang, S. V. Duy and S. Sauvé, Analysis of nine N-nitrosamines using liquid chromatography-accurate mass high resolution-mass spectrometry on a Q-Exactive instrument, *Anal. Methods*, 2015, **7**(14), 5748–5759, DOI: 10.1039/C4AY02967D.

33 C. Pu, B. R. Cavarra and T. Zeng, Combining High-Resolution Mass Spectrometry and Chemiluminescence Analysis to Characterize the Composition and Fate of Total N-Nitrosamines in Wastewater Treatment Plants, *Environ. Sci. Technol.*, 2024, **58**(38), 17081–17091, DOI: 10.1021/acs.est.4c06555.

34 G. Spedding, FULL CATALOG IS ON-LINE AT BDASTESTING.COM, 2022, Available from: https://bdastesting.com/wp-content/themes/mightily/pdf/Pricelist_BDASLLC_Updated2022.pdf.

35 Z. Guo, H. Feng and T. M. Swager, Reversible Electrochemical Sensor for NDMA: Leveraging Molecularly Imprinted Polymers for Enhanced Sensitivity and Selectivity, *ACS Sens.*, 2025, **10**(2), 881–885, DOI: 10.1021/acssensors.4c02462.

36 M. Valentino, A. Imbriano, A. Tricase, F. Della Pelle, D. Compagnone and E. Macchia, *et al.*, Electropolymerized molecularly imprinted polypyrrole film for dimethoate sensing: investigation on template removal after the imprinting process, *Anal. Methods*, 2023, **15**(10), 1250–1253, DOI: 10.1039/D2AY02024F.

37 T. W. von Zuben, A. G. Salles and J. A. Bonacin, Low-cost open-source potentiostats: A comprehensive review of DIY solutions and fundamental concepts of electronics and its integration with electrochemistry, *Electrochim. Acta*, 2024, **498**, 144619, DOI: 10.1016/j.electacta.2024.144619.

38 J. C. Beard, C. H. Wang, A. Sridharan, R. G. Croy, J. M. Essigmann and T. M. Swager, Colorimetric Detection of Aqueous *N*-Nitrosodimethylamine via Photonitrosation of a Naphtholsulfonate Indicator, *ACS Sens.*, 2024, **9**(9), 4655–4661, DOI: 10.1021/acssensors.4c00927.

39 C. E. Hefner, P. Aryal, E. Brack, T. Alexander and C. S. Henry, Capillary-flow driven microfluidic sensor based on tyrosinase for fast user-friendly assessment of pesticide exposures, *Analyst*, 2024, **149**(23), 5684–5692, DOI: 10.1039/D4AN01203H.

40 P. Aryal, E. Brack, T. Alexander and C. S. Henry, Capillary Flow-Driven Microfluidics Combined with a Paper Device for Fast User-Friendly Detection of Heavy Metals in Water, *Anal. Chem.*, 2023, **95**(13), 5820–5827, DOI: 10.1021/acs.analchem.3c00378.

41 I. Lewińska, P. Aryal, E. Brack and C. S. Henry, Capillary Flow-Driven, Disposable Device for Dissolved Oxygen Sensing in Water Samples, *Anal. Chem.*, 2025, **97**(45), 25078–25086, DOI: 10.1021/acs.analchem.5c03984.

42 C. Prakobdi, T. A. Baldo, P. Aryal, J. Link, P. Saetear and C. S. Henry, Non-invasive iron deficiency diagnosis: a saliva-based approach using capillary flow microfluidics, *Anal. Methods*, 2024, **16**(16), 2489–2495, DOI: 10.1039/D3AY01933K.

43 P. A. Pornchanok Punnoy, Smartphone-Assisted Dual-Sided Capillary Microfluidic Device for Multiplex Detection of Heavy Metals and Nutrients in Drinking Water, *Anal. Chim. Acta*, 2025, **1356**, 344031, DOI: 10.1016/j.aca.2025.344031.

44 P. Aryal, C. E. Hefner, B. Martinez, E. Brack and C. S. Henry, Citizen-Based Water Quality Monitoring: Field Testing a User-Friendly Sensor for Phosphate Detection in Global Surface Waters, *Anal. Chem.*, 2024, **96**(46), 18369–18376, DOI: 10.1021/acs.analchem.4c02123.

45 P. Aryal, A. W. Indrianingsih and C. S. Henry, Smartphone-enabled green anthocyanin sensor for Fe(III) sensing on paper using capillary-driven microfluidics, *Green Anal. Chem.*, 2024, **8**, 100091, DOI: 10.1016/j.greeac.2023.100091.

46 J. C. Beard and T. M. Swager, An organic chemist's guide to N-nitrosamines: their structure, reactivity, and role as contaminants, *J. Org. Chem.*, 2021, **86**(3), 2037–2057, DOI: 10.1021/acs.joc.0c02774.

47 P. Aryal, C. Hefner, B. Martinez and C. S. Henry, Microfluidics in environmental analysis: advancements, challenges, and future prospects for rapid and efficient monitoring, *Lab Chip*, 2024, **24**(5), 1175–1206, DOI: 10.1039/D3LC00871A.

48 LSU Macro, Whatman Filtration Product Guide, Available from: https://macro.lsu.edu/HowTo/Whatman-filtration-product-guide.pdf.

49 S. Richardson, A. Iles, J. M. Rotchell, T. Charlson, A. Hanson and M. Lorch, *et al.*, Citizen-led sampling to monitor phosphate levels in freshwater environments using a simple paper microfluidic device, *PLoS One*, 2021, **16**(12), e0260102.

50 Chromatographic Measurements, Part 5: Determining LOD and LOQ Based on the Calibration Curve | Separation Science, [cited 2025 Dec 24], Available from: https://www.sepscience.com/hplc-solutions-126-chromatographic-measurements-part-5-determining-lod-and-loq-based-on-the-calibration-curve-6959.

51 P. Aryal, J. Boes, E. Brack, T. Alexander and C. S. Henry, Fill, Fold, Photo: Preconcentration and Multiplex Detection of Trace Level Heavy Metals in Water, *ACS Sens.*, 2024, **9**(10), 5479–5488, DOI: 10.1021/acssensors.4c01708.

52 N. A. Meredith, J. Volckens and C. S. Henry, based microfluidics for experimental design: screening masking agents for simultaneous determination of Mn (II) and Co (II), *Anal. Methods*, 2017, **9**(3), 534–540, DOI: 10.1039/C6AY02798A.

53 F. Pena-Pereira, W. Wojnowski and M. Tobiszewski, AGREE—Analytical GREEnness metric approach and software, *Anal. Chem.*, 2020, **92**(14), 10076–10082, DOI: 10.1021/acs.analchem.0c01887.

54 AOAC International, Guidelines for Standard Method Performance Requirements (Appendix F), AOAC International, 2016, Available from: https://www.aoac.org/wp-content/uploads/2019/08/app_f.pdf.

